Hydrology and Earth System Sciences

Open Access

Discussions

Long-term and high frequency non-destructive monitoring of water stable isotope profiles in an evaporating soil column

Y. Rothfuss, S. Merz, J. Vanderborght, N. Hermes, A. Weuthen, A. Pohlmeier, H. Vereecken, and N. Brüggemann

Forschungszentrum Jülich GmbH, Institute of Bio- and Geosciences, Agrosphere Institute (IBG-3), Leo-Brandt-Straße, 52425 Jülich, Germany

Correspondence to: Y. Rothfuss (y.rothfuss@fz-juelich.de)

Printer-friendly Version

Interactive Discussion

Printer-friendly Version

Interactive Discussion

Abstract

The stable isotope compositions of soil water (δ^2H and δ^{18}O) carry important information about the prevailing soil hydrological conditions and for constraining ecosystem water budgets. However, they are highly dynamic, especially during and after precipitation events. The classical method of determining soil water δ^2H and δ^{18}O at different depths, i.e., soil sampling and cryogenic extraction of the soil water, followed by isotope-ratio mass spectrometer analysis is destructive and laborious with limited temporal resolution. In this study, we present a new non-destructive method based on gas-permeable tubing and isotope-specific infrared laser absorption spectroscopy. We conducted a laboratory experiment with an acrylic glass column filled with medium sand equipped with gas-permeable tubing at eight different soil depths. The soil column was initially saturated from the bottom, exposed to evaporation for a period of 290 days, and finally rewatered. Soil water vapor δ^2H and δ^{18}O were measured daily, sequentially for each depth. Soil liquid water δ^2H and δ^{18}O were inferred from the isotopic values of the vapor assuming thermodynamic equilibrium between liquid and vapor phases in the soil. The experimental setup allowed following the evolution of typical exponential-shaped soil water δ^2H and δ^{18}O profiles with unprecedentedly high temporal resolution. As the soil dried out, we could also show for the first time the increasing influence of the isotopically depleted ambient water vapor on the isotopically enriched liquid water close to the soil surface (i.e., atmospheric invasion). Rewatering at the end of the experiment led to instantaneous resetting of the stable isotope profiles, which could be closely followed with the new method.

1 Introduction

Stable isotopologues of water, namely ^{1}H^{2}H^{16}O and ^{1}H$_2$^{18}O are powerful tools used in a wide range of research disciplines at different and complementary temporal and spatial scales for, e.g., assessing the origin of water vapor (e.g., Craig, 1961; Liu et al.,

2010), solving water balances of lakes (Jasechko et al., 2013) and studying ground-water recharge (Blasch and Bryson, 2007; Peng et al., 2014). Analysis of the isotope compositions (δ^2H and δ^{18}O) of soil surface and leaf waters allows for partitioning evapotranspiration into evaporation and transpiration (e.g., Dubbert et al., 2013; Hu et al., 2014; Rothfuss et al., 2012; Yepez et al., 2005).

Moreover, from soil water δ^2H and δ^{18}O profiles, it is also possible to derive quantitative information, such as soil evaporation flux, locate evaporation fronts, and root water uptake depths (Rothfuss et al., 2010; Wang et al., 2010). Zimmermann et al. (1967) and later Barnes and Allison (1983, 1984) and Barnes and Walker (1989) first analytically described soil ^{1}H^{2}H^{16}O and ^{1}H$_2$^{18}O movement at steady/non-steady state and in isothermal/non-isothermal soil profiles. Between precipitation events, the soil water δ^2H and δ^{18}O profiles depend on flux boundary conditions, i.e., fractionating evaporation and non-fractionating capillary rise as well as on soil properties (e.g., soil tortuosity). In a saturated soil, the isotope excess at the surface due to evaporation diffuses back downwards, leading to typical and well documented exponential-shaped δ^2H and δ^{18}O profiles. For an unsaturated soil, assuming in a first approximation that isotope movement occurs in the vapor phase above the soil "evaporation front" (EF) and strictly in the liquid phase below it, the maximal δ^2H and δ^{18}O values are no longer observed at the surface but at the depth of EF. Above the EF, in the so-called "vapor region", by applying Fick's law, soil water δ^2H and δ^{18}O decrease towards the depleted ambient atmosphere water vapor δ^2H and δ^{18}O. Braud et al. (2005), Haverd and Cuntz (2010), Rothfuss et al. (2012), Singleton et al. (2004), and Sutanto et al. (2012) implemented the description of the transport of ^{1}H^{2}H^{16}O and ^{1}H$_2$^{18}O in physically based soil-vegetation-atmosphere transfer (SVAT) models (Hydrus 1D, SiSPAT-Isotope, Soil-Litter iso, TOUGHREACT). In these models, movement of soil ^{1}H^{2}H^{16}O and ^{1}H$_2$^{18}O occur in both phases below and above the EF, and heat and water transports are properly coupled.

However, these tools suffer from the comparison with other "traditional" methods developed to observe and derive soil water state and transport. In contrast with soil

Discussion Paper | Discussion Paper | Discussion Paper | Discussion Paper

water content and tension obtained by, e.g., time-domain reflectometry and tensiometry, isotope compositions are typically obtained following destructive sampling which greatly limits their informative value. Only since recently, non-destructive methodologies based on gas-permeable membrane and laser spectroscopy can be found in the literature (Rothfuss et al., 2013; Herbstritt et al., 2012; Volkmann and Weiler, 2014).

The central objective of this study was to demonstrate that a direct application of the method of Rothfuss et al. (2013) to a soil column would allow monitoring soil water δ^2H and δ^{18}O profiles in the laboratory with high temporal resolution and over a long time period. Furthermore, we aimed at demonstrating that the obtained isotope data can be used to locate the evaporation front as it recedes into the soil during the experiment.

2 Material and methods

2.1 Isotopic analyses

Isotopic analysis of liquid water and water vapor was performed using a cavity ring-down spectrometer (L1102-i, Picarro, Inc., Santa Clara, CA, USA), calibrated against the international primary water isotope standards V-SMOW2, GISP, and SLAP by liquid water injection into the vaporizer of the analyzer. Primary and working standards' isotope compositions were measured at 17 000 ppmv water vapor mixing ratio (number of replicates = 4, number of injections per replicate = 8). Average and SDs were calculated omitting the first three values of the first replicate to account for a potential memory effect of the laser spectrometer. The laser spectrometer's dependence on water vapor mixing ratio was also investigated according to the method of Schmidt et al. (2010). Hydrogen and oxygen isotope ratios of water are expressed in per mil (‰) on the international "delta" scale as defined by Gonfiantini (1978) and referred to as δ^2H and δ^{18}O, respectively.

2.2 Soil column and measurements

The experiment was conducted in a 0.0057 m^3 acrylic glass column (0.11 m i.d., 0.60 m height, Fig. 1a). The bottom of the column consisted of a porous glass plate (10 µm < pore size diameter < 16 µm (4th class), Robu$^®$ GmbH, Hattert, Germany) connected to a two-way manual valve (VHK-2-01S-06F, SMC Pneumatik GmbH, Germany).

Three ports were available at each of eight different depths (–0.01, –0.03, –0.05, –0.07, –0.10, –0.20, –0.40, and –0.60 m): one inlet for the carrier gas, i.e., synthetic dry air (20.5 % O$_2$ in N$_2$, with approx. 20–30 ppmv water vapor; Air Liquide, Germany), one sample air outlet, and one duct for a soil temperature (T_S) sensor (type K thermocouple, Greisinger electronic GmbH, Regenstauf, Germany; precision: 0.1 °C). An additional fourth port at depths –0.01, –0.03, –0.05, –0.10, –0.20, and –0.60 m was used for the measurement of soil volumetric water content (θ) (EC-5, Decagon Devices, USA; precision: 0.02 m^3 m^{-3}).

At each depth inside the column a 0.15 m long piece of microporous polypropylene tubing (Accurel$^®$ PP V8/2HF, Membrana GmbH, Germany; 0.155 cm wall thickness, 0.55 cm i.d., 0.86 cm o.d.) was connected to the gas inlet and outlet port. The tubing offers the two advantages of being gas-permeable (pore size of 0.2 µm) and exhibiting strong hydrophobic properties to prevent liquid water from intruding into it. It allows sampling of soil water vapor and, hence, the determination of the isotope composition of soil liquid water (δ_S) in a non-destructive manner considering thermodynamic equilibrium between liquid and vapor phases as detailed by Rothfuss et al. (2013).

2.3 Internal isotope standards

Two internal standards ("st1" and "st2") were prepared using the same procedure as described by Rothfuss et al. (2013). Two acrylic glass vessels (0.122 m i.d., 0.22 m height), in each of which a 0.15 m long piece of tubing as well as a type K thermocouple were installed, were filled with FH31 sand (porosity = 0.34 m^3 m^{-3}, dry bulk density = 1.69 g cm^3, particle size distribution: 10 % (> 0.5 mm), 72 % (0.25–0.5 mm), and 18 %

(< 0.25 mm)) (Merz et al., 2014; Stingaciu et al., 2009). Each vessel was saturated with water of two different isotope compositions: $\delta^2 H_{st1} = -53.51(\pm0.10)$‰, $\delta^{18}O_{st1} = -8.18(\pm0.06)$‰ and $\delta^2 H_{st2} = +15.56(\pm0.12)$‰, $\delta^{18}O_{st2} = +8.37(\pm0.04)$‰. Soil water vapor from each vessel was sampled eight times per day for 30 min during the whole experiment.

2.4 Atmospheric measurements

Laboratory air was sampled at 2 m above the sand surface for isotope analysis of water vapor (δ_a). Air relative humidity (RH) and temperature (T_a) were monitored at the same height with a combined RH and T_a sensor (RFT-2, UMS GmbH, Germany; precision for RH and T_a were 2 % and 0.1° C, respectively). Vapor pressure deficit (vpd) was calculated from RH and T_a data using the Magnus–Tetens formula (Murray, 1967) for saturated vapor pressure. The laboratory was air-conditioned and ventilated with seven axial fans (ETRI 148VK0281, 117 L s^{-1} airflow, ETRI/Rosenberg, USA) positioned at 1.80 m height above the sand surface.

2.5 Sampling protocol and applied isotopic calibrations

The column was filled in a single step with FH31 sand and carefully shaken in order to reach a dry bulk density close to in situ field conditions. The sand was then slowly saturated from the bottom from an external water tank filled with st1 water on 2 December 2013. After saturation, the column was disconnected and sealed at the bottom using the two-way manual valve. It was finally installed on a balance (Miras 2 – 60EDL, Sartorius, USA), and let to evaporate for a period of 290 days.

δ_S was determined in a sequential manner at each available depth once a day following the method developed by Rothfuss et al. (2013) (Fig. 1b). Dry synthetic air at a rate of 50 mL min^{-1} from a mass flow controller (EL-FLOW Analog, Bronkhorst High Tech, Ruurlo, the Netherlands) was directed to the permeable tubing for 30 min at each depth. The sampled soil water vapor was diluted with dry synthetic air provided by a second

mass flow controller of the same type in order to (i) reach a water vapor mixing ratio value ranging between 17 000 and 23 000 ppmv (where L1102-i isotope measurements are most precise) and (ii) generate an excess flow downstream of the laser analyzer to avoid any contamination of sample air with ambient air. The excess flow was measured with a digital flow meter (ADM3000, Agilent Technologies, Santa Clara, CA, USA). The last 100 observations (corresponding to approx. 10 min) at steady state (SDs < 0.70 ‰ and < 0.20 ‰ for δ^2H and δ^{18}O, respectively) were used to calculate the raw isotope compositions of soil water vapor (δ_{Svap}), correcting for the water vapor mixing ratio dependence of the laser analyzer readings with 17 000 ppmv as reference level. Finally, these corrected values were used to infer the corresponding δ_S at the measured T_S (Eqs. 1 and 2; taken from Rothfuss et al., 2013):

$$\delta^2H_S = 104.96 - 1.0342 \cdot T_S + 1.0724 \cdot \delta^2H_{Svap} \tag{1}$$

$$\delta^{18}O_S = 11.45 - 0.0795 \cdot T_S + 1.0012 \cdot \delta^{18}O_{Svap} \tag{2}$$

The isotope composition of laboratory water vapor (δ_a) was measured eight times a day. δ_a and δ_S values were finally corrected for laser instrument drift with time, using the isotope compositions of the two water standards, δ_{st1} and δ_{st2}.

Water vapor of the ambient air, of both standards, and from the different tubing sections in the soil column were sampled sequentially in the following order: soil (0.60 m) – soil (0.40 m) – atmosphere – st1 – st2 – soil (0.20 m) – soil (0.10 m) – atmosphere – st1 – st2 – soil (0.07 m) – soil (0.05 m) – atmosphere – st1 – st2 – soil (0.03 m) – soil (0.01 m). Atmosphere water vapor was sampled twice as long (i.e., one hour) as soil water vapor from the column/standards so that each sequence lasted exactly 10 h and started each day at the same time. The remaining 14 h were used for additional standard and atmosphere water vapor measurements (i.e., on five occasions each).

2.6 Irrigation event

On Day of Experiment (DoE) 290 at 09:30 UTC+02:00 the sand surface was irrigated with 70 mm of st1 water over one hour in order to avoid oversaturation of the sand and

avoid preferential pathways that would have affected the evaporation rate. For this, a 2 L polyethylene bottle was used. Its bottom was perforated with a set of 17 holes of 5 mm diameter and its cap with a single hole through which a PTFE bulkhead union tube fitting (Swagelok, USA) was installed. The bulkhead fitting was connected to a two-way needle valve (Swagelok, USA) for adjusting the irrigation flow rate.

To better observe the dynamics directly following the irrigation event, water vapor was sampled at a higher rate, i.e., 1, 3, 4, 5, 6, 9, 11, and 11 times per day at −0.60, −0.40, −0.20, −0.10, −0.07, −0.05, −0.03, and −0.01 m. Water vapor from both standards was sampled twice a day. The experiment was terminated after 299 days on 26 September 2014.

3   Results

3.1   Example of a measuring sequence

Figure 2 shows exemplarily the measuring sequence for DoE 150. Soil and standards water vapor mixing ratios were stable and ranged between 17 200 and 18 200 ppmv during the last 10 min of each sampling period (Fig. 2a). δ_{Svap} was within the range spanned by δ_{st1vap} and δ_{st2vap} for both ^{2}H and ^{18}O (Fig. 2b). On DoE 150, the soil surface was sufficiently dry so that atmospheric invasion of water vapor had started to significantly influence the δ_{Svap} of the upper soil layers. Therefore, δ_{Svap} measured at −0.01 m was lower than at −0.03 m for both ^{2}H and ^{18}O, but less pronounced for ^{2}H.

3.2   Time courses of air temperature, relative humidity and atmospheric δ^2H and δ^{18}O

During the experiment, the laboratory air temperature ranged from 15.6 to 22.5 °C (average: 18.7 ± 1.5 °C, Fig. 3a) and the relative humidity from 19 to 69 % (average: 40 % ± 0.08 %, Fig. 3a). Lower values of δ_a were observed from DoE 0 to 125 at lower

Full Screen / Esc

Printer-friendly Version

Interactive Discussion

air temperatures, whereas higher values occurred after DoE 125 at higher air temperatures (Fig. 3b).

3.3 Evolution of soil water content, temperature, evaporation flux, and δ_{Svap} from DoE 0–290

The soil temperature ranged from 16.2 to 22.3 °C (average: 18.6 ± 1.3 °C, data not shown) and closely followed that in the air, i.e., differences between daily mean soil and air temperatures ranged from −0.2 to 0.2 °C during the experiment. Following the saturation of the column, a strong decrease in water content was observed in the upper 10 cm, whereas after 287 days the sand was still saturated at −0.60 m (Fig. 4a). Figure 4b shows the time series of evaporation flux normalized by the vapor pressure deficit in the laboratory air (Ev/vpd, expressed in mm day^{-1} kPa^{-1}). Ev/vpd ratio was high at the beginning of the experiment, i.e., ranged from 2.44 to 3.22 mm d^{-1} kPa^{-1} during the first two experimental days. After DoE 180 and until the soil was irrigated, Ev/vpd stabilized to a mean value of 0.03(±0.02) mm d^{-1} kPa^{-1}.

Due to fractionating evaporation flux, the δ_{Svap} of the topmost layer (−0.01 m) increased instantaneously (i.e., from DoE 0 onward) from the equilibrium δ_{Svap} value with the input water (−17.3 and −132.3 ‰ for ^{18}O and ^{2}H, respectively, at 16.5 °C, Fig. 4c and d). Through back-diffusion of the excess heavy stable isotopologues from the evaporation front, δ_{Svap} measured at depths −0.03, −0.05, −0.07, −0.10, and −0.20 m departed from that same equilibrium value after 2, 3, 10, 25, and 92 days of the experiment, respectively. On the other hand, δ_{Svap} of the layers −0.40 and −0.60 m were constant over the entire duration of the experiment. Until DoE 65, the δ_{Svap} of the first 10 cm increased. From DoE 65 to 113 δ_{Svap} reached an overall stable value in the top layers −0.01 m (δ^{2}H$_{Svap}$ = 4.82 ± 2.06 ‰; δ^{18}O$_{Svap}$ = 11.72 ± 0.67 ‰) and −0.03 m (δ^{2}H$_{Svap}$ = 5.61±3.14 ‰; δ^{18}O$_{Svap}$ = 10.41±0.81 ‰), whereas δ_{Svap} measured at depths −0.05, −0.07, and −0.10 m still progressively increased; from DoE 72 onward, δ_{Svap} at −0.20 m started to increase. δ^{2}H$_{Svap}$ and δ^{18}O$_{Svap}$ values started to decrease

after about DoE 113 and DoE 155, respectively. $\delta^2 H_{Svap}$ at –0.01, –0.03, and –0.07 m on the one hand and $\delta^{18}O_{Svap}$ at –0.01, –0.03, and –0.07 m on the other followed similar evolutions with maximum values measured below the surface down to –0.05 m.

3.4 Evolution of soil water content, temperature, evaporation flux, and δ_{Svap} from DoE 290 to 299

The layers –0.01, –0.03, –0.05, –0.10, and –0.20 m showed increases in θ of 0.31, 0.22, 0.30, 0.23, and 0.16 $m^3 m^{-3}$ following irrigation, whereas θ at –0.60 m remained constant (Fig. 4e). $\theta_{-0.01\,m}$ and $\theta_{-0.03\,m}$ rapidly decreased down to values of 0.12 and 0.13 $m^3 m^{-3}$. Note that when $\theta_{-0.01\,m}$ and $\theta_{-0.03\,m}$ reached these values prior to irrigation, the evaporation rate was similar (i.e., Ev/vpd = 0.65(±0.12) $mm\,d^{-1}$, Fig. 4f).

Immediately after irrigation and for both isotopologues, δ_{Svap} at –0.01, –0.03, and –0.05 m was reset to a value close to that in equilibrium with st1 water (i.e., –17.8‰ and –132.0‰ for ^{18}O and ^2H, respectively, at 21.8 °C soil temperature, Fig. 4g and h). At –0.07 m, δ_{Svap} reached the above mentioned equilibrium values after about 3.5 days. δ_{Svap} at –0.20 m evolved in a similar way, whereas at –0.10 m the equilibrium values were reached after six hours. Finally, δ_{Svap} at –0.40 and –0.60 m and for both isotopologues were not affected by the water addition, which was consistent with the observed θ changes.

3.5 Evolution of soil temperature, water content, and δ_S profiles

In Fig. 5, T_S, θ, and δ_S profiles for both isotopologues are plotted in three different panels, from DoE 0 to 100 (Fig. 5a–d, top panels), from DoE 101 to 287 (Fig. 5e–h, center panels), and from DoE 288 to 299 (Fig. 5i–l, bottom panels). The represented profiles were obtained from a linear interpolation of the times series of each variable. Thus, since the measuring sequence started each day at 08:00 and ended at 18:00, the depicted profiles are centered on 13:00.

Even if the soil temperature fluctuated during the course of the experiment, quasi-isothermal conditions were fulfilled at a given date, as the column was not isolated from its surroundings. On average, T_S only varied by 0.2 °C around the profile mean temperature at a given date. The δ_S profiles showed a typical exponential shape from DoE 0 to approx. 100. Around DoE 100, when θ at −0.01 m reached a value of 0.090 m³ m⁻³ (i.e., significantly greater than the sand residual water content θ = 0.035 m³ m⁻³, determined by Merz et al., 2014), the maximal δ_S values were no longer observed at the surface and atmosphere water vapor started invading the first centimeter of soil. Note that this happened slightly faster for $^1H^2H^{16}O$ than for $^1H_2^{18}O$. On DoE 290, when the column was irrigated, the isotope profiles were partly reset to their initial state, i.e., constant over depth and close to −53.5 and −8.2 ‰ for $^1H^2H^{16}O$ and $^1H_2^{18}O$, respectively, with the exception of still enriched values at −0.07 m.

4   Discussion

4.1   Long term reliability of the method

The method proved to be reliable in the long term as the tubing sections positioned at −0.60 and −0.40 m (i.e., where the sand was saturated or close to saturation during the entire experiment) remained watertight even after 299 days. As demonstrated by Rothfuss et al. (2013), (i) the length of the gas-permeable tubing, (ii) the low synthetic dry air flow rate, and (iii) the daily measurement frequency allowed removing soil water vapor which remained under thermodynamic equilibrium with the soil moisture. Moreover, this was also true for the upper soil layers even at very low soil water content: steady values for water vapor mixing ratio and isotope compositions were always reached during sampling throughout the experiment. Finally, our method enabled inferring the isotope composition of very tightly bound water at the surface, which would be observable by the traditional vacuum distillation method with certainly a lower vertical resolution due to very low moisture content. As also pointed out by Rothfuss et al. (2013), it can be

assumed that the sand properties did not cause any fractionation of pore water ^{2}H and ^{18}O. In contrast, this could not be the case in certain soils with high cation exchange capacity (CEC) as originally described by Sofer and Gat (1972) and recently investigated by Oerter et al. (2014).

4.2 δ^2H–δ^{18}O relationships in soil water and atmosphere water vapor

Each plot of Fig. 6 represents data of 50 consecutive days of the experiment. Atmosphere water vapor δ^2H and δ^{18}O (gray symbols) were linearly correlated (linear regression relationships in gray dotted lines) during the entire experiment (R^2 ranging between 0.7 and 0.9), with the exception of the period DoE 125–155, when atmospheric δ^2H was remarkably high in the laboratory (Fig. 6c and d).

The linear regression slopes (LRS) between δ^2H$_a$ and δ^{18}O$_a$ ranged from 6.20 (DoE 50–100) to 8.29 (DoE 0–50, gray dotted line). These values were significantly lower than the calculated ratio of the equilibrium fractionation for ^{1}H^{2}H^{16}O and ^{1}H$_2$^{18}O that characterizes meteoric water bodies, which should have ranged between 8.32 (DoE 200–250) and 8.47 (DoE 0–50) at the measured laboratory air temperatures. Therefore, it can be deduced that the laboratory air moisture was partly resulting from column evaporation, typically leading to a δ^2H–δ^{18}O regression slope of lower than eight.

Considering all soil depths, the δ^2H$_S$–δ^{18}O$_S$ LRS increased from 2.96 to 4.86 over the course of the experiment (with $R^2 > 0.89$). However, Fig. 6 highlights the fact that in the upper three layers (–0.01, –0.03, and –0.05 m) δ^2H$_S$–δ^{18}O$_S$ LRS followed a significantly different evolution as the soil dried out. Figure 7 shows average δ^2H–δ^{18}O LRS calculated for time intervals of ten consecutive days for the atmosphere (gray line), the three upper layers (colored solid lines), and the remaining deeper layers (–0.07, –0.10, –0.20, –0.40, and –0.60 m, black dotted line). While both δ^2H–δ^{18}O LRS in the atmosphere and in the first three depths fluctuated during the experiment, the LRS of the combined remaining deeper layers varied only little between 3.07 and 4.49 (average = 3.78 ± 0.54). From DoE 150, δ^2H–δ^{18}O LRS of the atmosphere and at –0.01, –0.03,

and −0.05 m were linearly correlated (R^2 = 0.73, 0.48, and 0.42, respectively), whereas they were not correlated before DoE 125, demonstrating again the increasing influence of the atmosphere (atmosphere invasion) on the soil surface layer as the EF receded in the soil. Note the absence of $\delta^2 H_a$−$\delta^{18}O_a$ linear correlation (LRS < 0, with negative R^2) observed between DoE 125 and 150, due to remarkably high atmosphere vapor $\delta^2 H$ measured in the laboratory.

4.3 Locating the evaporation front depth from soil water $\delta^2 H$ and $\delta^{18}O$ profiles

From Fig. 4b no distinct characteristic evaporation stages, i.e., stages I and II referring to atmosphere-controlled and soil-controlled evaporation phases, respectively, could be identified as opposed to Merz et al. (2014), who conducted an evaporation study using the same sand. This indicates greater wind velocity in the air layer above the soil column due to the laboratory ventilation system which would lead to a decrease in evaporation rate during stage I due to an increased transfer resistance in the boundary layer above the drying porous medium as observed and modelled by Shahraeeni et al. (2012).

Locating the EF in the soil is of importance for evapotranspiration partitioning purposes: from the soil water isotope composition at the EF, it is possible to calculate the evaporation flux isotope composition using the Craig and Gordon formula (Craig and Gordon, 1965). For a uniform isotope diffusion coefficient distribution in the liquid phase, an exponential decrease of the isotope composition gradient with depth is expected. However, when evaporation and thus accumulation of isotopologues occur in a soil layer between two given observation points, then the isotope gradient between these two points is smaller than the gradient deeper in the profile. Therefore we can consider the time when the isotope composition gradient is no longer the largest between these two upper observation depths as the time when the EF moves into the soil layer below.

Figure 8a and b display the evolutions of the isotope compositions gradients $\mathrm{d}(\delta^{18}\mathrm{O_S})/\mathrm{d}z$ and $\mathrm{d}(\delta^2\mathrm{H_S})/\mathrm{d}z$ calculated between two consecutive observation points in the soil (i.e., between −0.01 and −0.03 m in brown solid line, between −0.03 and −0.05 m in red solid line, etc.). Figure 8c translates these isotope gradients in terms of EF depths ($z^{18}\mathrm{O_{EF}}$ and $z^2\mathrm{H_{EF}}$, respectively). Each day, the maximum $\mathrm{d}(\delta^{18}\mathrm{O_S})/\mathrm{d}z$ and $\mathrm{d}(\delta^2\mathrm{H_S})/\mathrm{d}z$ define the layer where evaporation occurs, e.g., when $\mathrm{d}(\delta^{18}\mathrm{O_S})/\mathrm{d}z$ is maximal between −0.01 and −0.03 m on a given DoE, $z^{18}\mathrm{O_{EF}}$ is estimated to be greater than −0.01 m and is assigned the value of 0 m. When $\mathrm{d}(\delta^{18}\mathrm{O_S})/\mathrm{d}z$ is maximal between −0.03 and −0.05 m on a given DoE, $z^{18}\mathrm{O_{EF}}$ is estimated to range between than −0.01 and −0.03 m and is assigned the value −0.02 m. From both $\mathrm{d}(\delta^{18}\mathrm{O_S})/\mathrm{d}z$ and $\mathrm{d}(\delta^2\mathrm{H_S})/\mathrm{d}z$, a similar evolution of the depth of the evaporation front was derived despite the fact that $\delta^2\mathrm{H_S}$ and $\delta^{18}\mathrm{O_S}$ time courses were different and showed maxima at different times. It was inferred that after 290 days under the prevailing laboratory air temperature, moisture, and aerodynamic conditions, and given the specific hydraulic properties of the sand, the EF had moved down to an approximate depth of −0.06 m.

5 Conclusion

Since the initial work of Zimmermann et al. (1967), water stable isotopologues have proven both theoretically and experimentally to be valuable tools for the study of water flow in the soil and at the soil–atmosphere interface. In this work we present a novel approach based on gas-permeable tubing and isotope-specific infrared laser absorption spectroscopy which allows overcoming limitations due to destructive sampling and offline isotope analysis leading to an insufficient time resolution.

Our newly developed method proved to be reliable over long time periods and followed quantitatively the progressive isotope enrichment caused by evaporation in an initially saturated soil column. Moreover, it could capture sudden variations following a simulated intense rain event. Our method will allow experimentalists to measure and

locate the evaporation front in a dynamic and non-destructive manner and to calculate the isotope compositions of the evaporation flux using the model of Craig and Gordon (1965) with much higher time resolution. Provided that the isotope compositions of evapotranspiration and transpiration fluxes are measured or modelled, this method will be especially useful to test hypotheses and improve our understanding of root water uptake processes and the partitioning of evapotranspiration fluxes.

References

Barnes, C. J. and Allison, G. B.: The distribution of deuterium and O-18 in dry soils. 1. Theory, J. Hydrol., 60, 141–156, doi:10.1016/0022-1694(83)90018-5, 1983.

Barnes, C. J. and Allison, G. B.: The distribution of deuterium and O-18 in dry soils. 3. Theory for non-isothermal water-movement, J. Hydrol., 74, 119–135, doi:10.1016/0022-1694(84)90144-6, 1984.

Barnes, C. J. and Walker, G. R.: The distribution of deuterium and O-18 during unsteady evaporation from a dry soil, J. Hydrol., 112, 55–67, doi:10.1016/0022-1694(89)90180-7, 1989.

Blasch, K. W. and Bryson, J. R.: Distinguishing sources of ground water recharge by using delta H-2 and delta O-18, Ground Water, 45, 294–308, doi:10.1111/j.1745-6584.2006.00289.x, 2007.

Full Screen / Esc

Printer-friendly Version

Interactive Discussion

Braud, I., Bariac, T., Gaudet, J. P., and Vauclin, M.: SiSPAT-Isotope, a coupled heat, water and stable isotope (HDO and (H2O)-O-18) transport model for bare soil. Part I. Model description and first verifications, J. Hydrol., 309, 277–300, doi:10.1016/j.jhydrol.2004.12.013, 2005.

Craig, H.: Isotopic variations in meteoric waters, Science, 133, 1702–1703, doi:10.1126/science.133.3465.1702, 1961.

Craig, H. and Gordon, L. I.: Deuterium and oxygen 18 variations in the ocean and marine atmosphere, in: Stable Isotopes in Oceanographic Studies and Paleotemperatures, Spoleto, Italy, 9–130, 1965.

Dubbert, M., Cuntz, M., Piayda, A., Maguás, C., and Werner, C.: Partitioning evapotranspiration – testing the Craig and Gordon model with field measurements of oxygen isotope ratios of evaporative fluxes, J. Hydrol., 496, 142–153, doi:10.1016/j.jhydrol.2013.05.033, 2013.

Gonfiantini, R.: Standards for stable isotope measurements in natural compounds, Nature, 271, 534–536, 1978.

Haverd, V. and Cuntz, M.: Soil-Litter-Iso: a one-dimensional model for coupled transport of heat, water and stable isotopes in soil with a litter layer and root extraction, J. Hydrol., 388, 438–455, doi:10.1016/j.jhydrol.2010.05.029, 2010.

Herbstritt, B., Gralher, B., and Weiler, M.: Continuous in situ measurements of stable isotopes in liquid water, Water Resour. Res., 48, W03601, doi:10.1029/2011wr011369, 2012.

Hu, Z. M., Wen, X. F., Sun, X. M., Li, L. H., Yu, G. R., Lee, X. H., and Li, S. G.: Partitioning of evapotranspiration through oxygen isotopic measurements of water pools and fluxes in a temperate grassland, J. Geophys. Res.-Biogeo., 119, 358–371, doi:10.1002/2013jg002367, 2014.

Jasechko, S., Sharp, Z. D., Gibson, J. J., Birks, S. J., Yi, Y., and Fawcett, P. J.: Terrestrial water fluxes dominated by transpiration, Nature, 496, 347–350, doi:10.1038/Nature11983, 2013.

Liu, Z. F., Bowen, G. J., and Welker, J. M.: Atmospheric circulation is reflected in precipitation isotope gradients over the conterminous United States, J. Geophys. Res.-Atmos., 115, D22120, doi:10.1029/2010jd014175, 2010.

Merz, S., Pohlmeier, A., Vanderborght, J., van Dusschoten, D., and Vereecken, H.: Moisture profiles of the upper soil layer during evaporation monitored by NMR, Water Resour. Res., 50, 5184–5195, doi:10.1002/2013wr014809, 2014.

Murray, F. W.: On the computation of saturation vapor pressure, J. Appl. Meteorol., 6, 203–204, 1967.

Oerter, E., Finstad, K., Schaefer, J., Goldsmith, G. R., Dawson, T., and Amundson, R.: Oxygen isotope fractionation effects in soil water via interaction with cations (Mg, Ca, K, Na) adsorbed to phyllosilicate clay minerals, J. Hydrol., 515, 1–9, doi:10.1016/j.jhydrol.2014.04.029, 2014.

Peng, T. R., Lu, W. C., Chen, K. Y., Zhan, W. J., and Liu, T. K.: Groundwater-recharge connectivity between a hills-and-plains' area of western Taiwan using water isotopes and electrical conductivity, J. Hydrol., 517, 226–235, doi:10.1016/j.jhydrol.2014.05.010, 2014.

Phillips, D. L. and Gregg, J. W.: Uncertainty in source partitioning using stable isotopes, Oecologia, 127, 171–179, doi:10.1007/s004420000578, 2001.

Rothfuss, Y., Biron, P., Braud, I., Canale, L., Durand, J. L., Gaudet, J. P., Richard, P., Vauclin, M., and Bariac, T.: Partitioning evapotranspiration fluxes into soil evaporation and plant transpiration using water stable isotopes under controlled conditions, Hydrol. Process., 24, 3177–3194, doi:10.1002/Hyp.7743, 2010.

Rothfuss, Y., Braud, I., Le Moine, N., Biron, P., Durand, J. L., Vauclin, M., and Bariac, T.: Factors controlling the isotopic partitioning between soil evaporation and plant transpiration: assessment using a multi-objective calibration of SiSPAT-Isotope under controlled conditions, J. Hydrol., 442, 75–88, doi:10.1016/j.jhydrol.2012.03.041, 2012.

Rothfuss, Y., Vereecken, H., and Brüggemann, N.: Monitoring water stable isotopic composition in soils using gas-permeable tubing and infrared laser absorption spectroscopy, Water Resour. Res., 49, 1–9, doi:10.1002/wrcr.20311, 2013.

Schmidt, M., Maseyk, K., Lett, C., Biron, P., Richard, P., Bariac, T., and Seibt, U.: Concentration effects on laser-based δ^{18}O and δ^2H measurements and implications for the calibration of vapour measurements with liquid standards, Rapid Commun. Mass Sp., 24, 3553–3561, doi:10.1002/rcm.4813, 2010.

Shahraeeni, E., Lehmann, P., and Or, D.: Coupling of evaporative fluxes from drying porous surfaces with air boundary layer: characteristics of evaporation from discrete pores, Water Resour. Res., 48, W09525, doi:10.1029/2012wr011857, 2012.

Singleton, M. J., Sonnenthal, E. L., Conrad, M. E., DePaolo, D. J., and Gee, G. W.: Multiphase reactive transport modeling of seasonal infiltration events and stable isotope fractionation in unsaturated zone pore water and vapor at the Hanford site, Vadose Zone J., 3, 775–785, 2004.

Sofer, Z. and Gat, J. R.: Activities and concentrations of O-18 in concentrated aqueous salt solutions – analytical and geophysical implications, Earth Planet. Sc. Lett., 15, 232–238, doi:10.1016/0012-821x(72)90168-9, 1972.

Stingaciu, L. R., Pohlmeier, A., Blumler, P., Weihermuller, L., van Dusschoten, D., Stapf, S., and Vereecken, H.: Characterization of unsaturated porous media by high-field and low-field NMR relaxometry, Water Resour. Res., 45, W08412, doi:10.1029/2008wr007459, 2009.

Sutanto, S. J., Wenninger, J., Coenders-Gerrits, A. M. J., and Uhlenbrook, S.: Partitioning of evaporation into transpiration, soil evaporation and interception: a comparison between iso-tope measurements and a HYDRUS-1D model, Hydrol. Earth Syst. Sci., 16, 2605–2616, doi:10.5194/hess-16-2605-2012, 2012.

Volkmann, T. H. M. and Weiler, M.: Continual in situ monitoring of pore water stable isotopes in the subsurface, Hydrol. Earth Syst. Sci., 18, 1819–1833, doi:10.5194/hess-18-1819-2014, 2014.

Wang, P., Song, X. F., Han, D. M., Zhang, Y. H., and Liu, X.: A study of root water uptake of crops indicated by hydrogen and oxygen stable isotopes: a case in Shanxi Province, China, Agr. Water Manage., 97, 475–482, doi:10.1016/j.agwat.2009.11.008, 2010.

Yepez, E. A., Huxman, T. E., Ignace, D. D., English, N. B., Weltzin, J. F., Castellanos, A. E., and Williams, D. G.: Dynamics of transpiration and evaporation following a moisture pulse in semiarid grassland: a chamber-based isotope method for partitioning flux components, Agr. Forest Meteorol., 132, 359–376, doi:10.1016/j.agrformet.2005.09.006, 2005.

Zimmermann, U., Ehhalt, D., and Münnich, K. O.: Soil Water Movement and Evapotranspiration: Changes in the Isotopic Composition of the Water, Symposium of Isotopes in Hydrology, 14–18 November 1966, Vienna, 567–584, 1967.

Title Page

Abstract | Introduction

Conclusions | References

Tables | Figures

◀ | ▶

◀ | ▶

Back | Close

Full Screen / Esc

Printer-friendly Version

Interactive Discussion
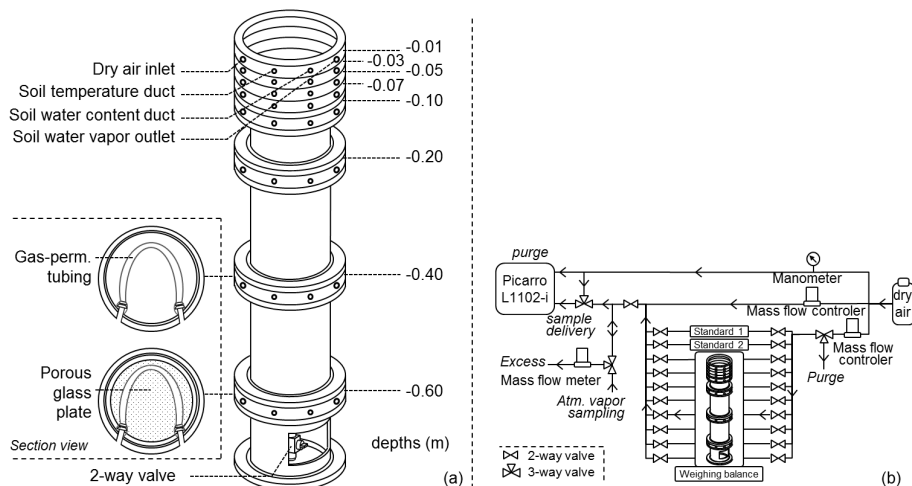
Figure 1. (a) Scheme of the acrylic glass column used in the experiment; **(b)** experimental setup for sampling water vapor at the different soil depths of the soil column, from the ambient air, and from the two soil water standards (standard 1 and 2).

Title Page

Abstract | Introduction

Conclusions | References

Tables | Figures

|◄ | ►|

◄ | ►

Back | Close

Full Screen / Esc

Printer-friendly Version

Interactive Discussion
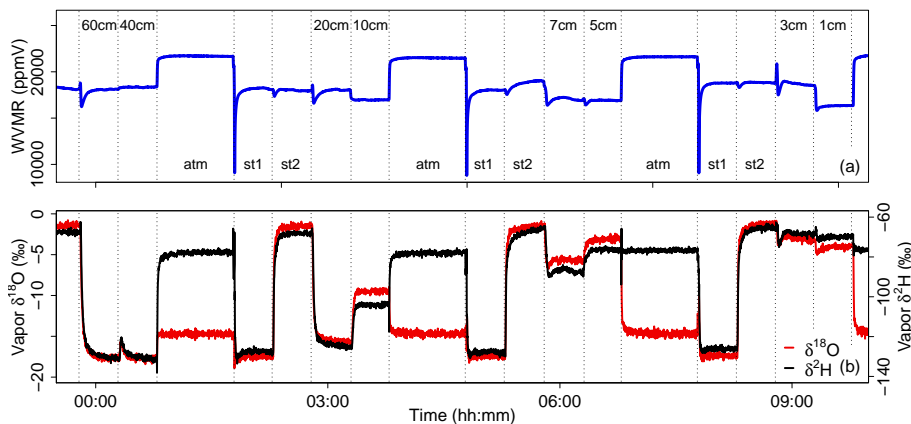
Figure 2. Water vapor mixing ratio (WVMR, in ppmv) and isotope composition (δ^{18}O and δ^2H, in ‰ V-SMOW) of the water vapor sampled on Day of Experiment 150 from the ambient air ("atm"), both standards ("st1" and "st2"), and from the tubing sections at soil depths 1, 3, 5, 7, 10, 20, 40, and 60 cm.
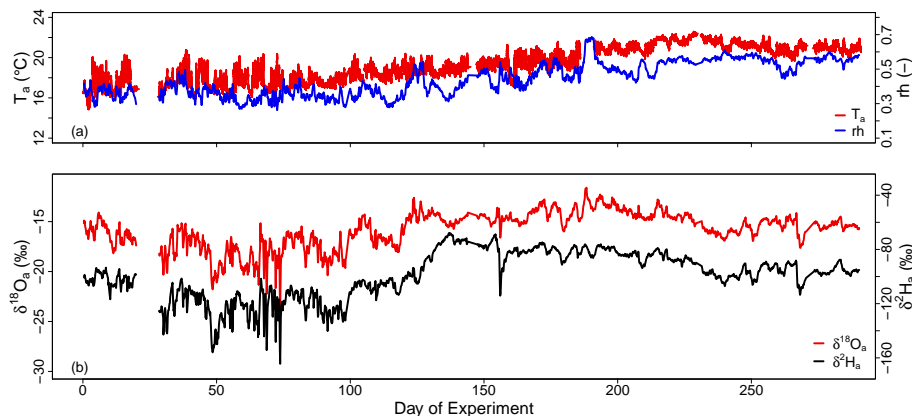
Figure 3. Time series of the laboratory ambient air temperature (T_a, in ˚C), relative humidity (RH, in %) and water vapor isotope compositions ($\delta^{18}O_a$ and δ^2H_a, in ‰ V-SMOW) over the course of the experiment.
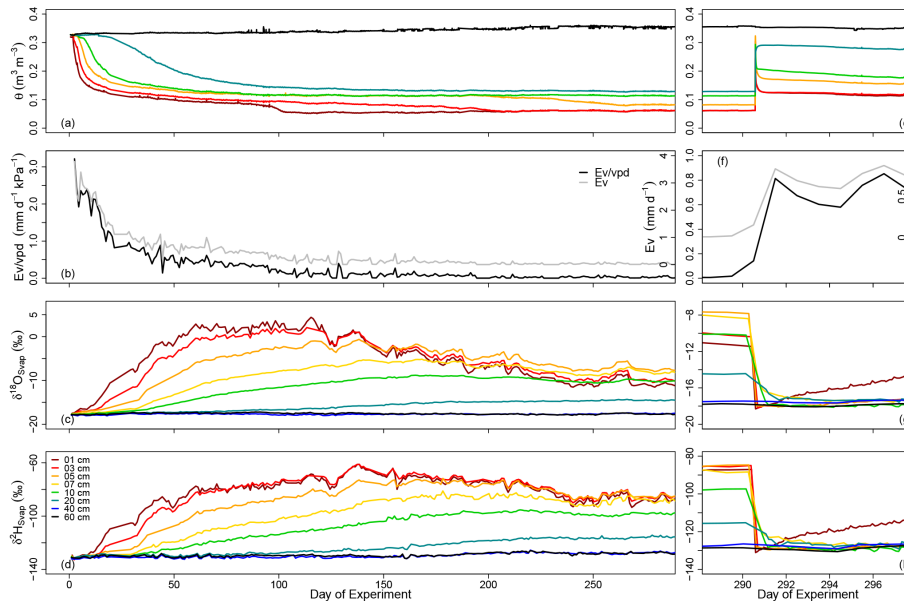
Figure 4. Time series of soil temperature (T_S, in ˚C), water content (θ, in $m^3\,m^{-3}$), evaporation flux (Ev, in $mm\,d^{-1}$), and water vapor isotope compositions ($\delta^{18}O_{Svap}$ and δ^2H_{Svap}, in ‰ V-SMOW) during the course of the experiment.
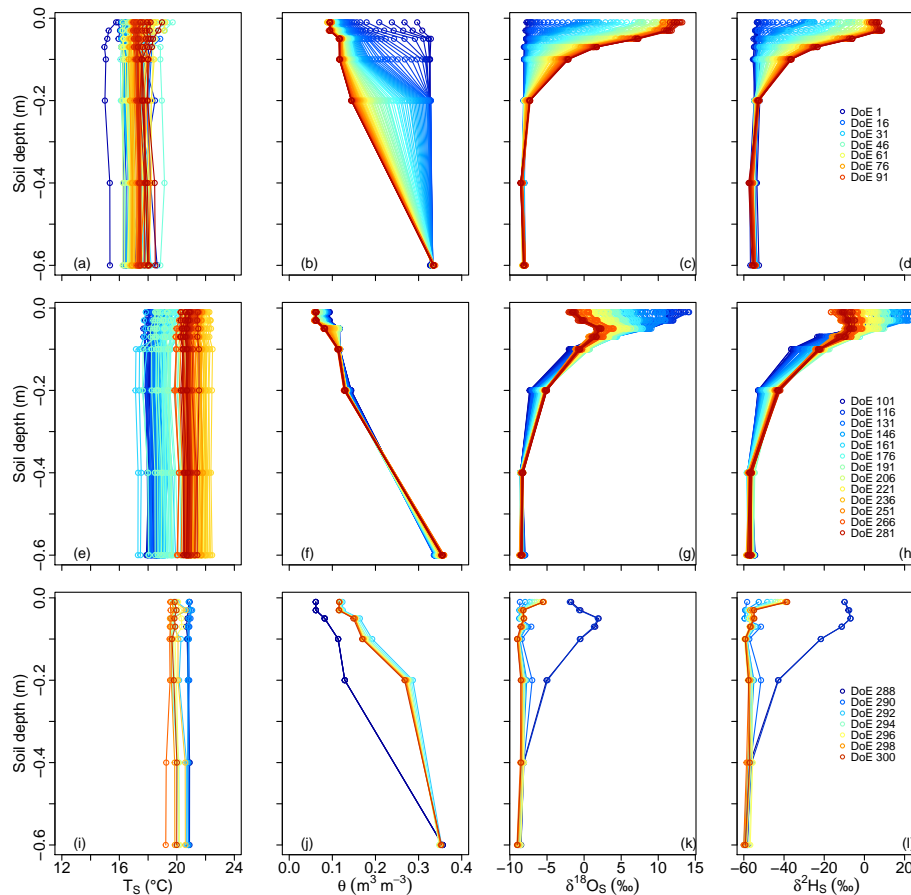
Figure 5. Soil temperature (T_S, in °C), water content (θ, in $m^3\,m^{-3}$), and liquid water isotope compositions ($\delta^{18}O_S$ and δ^2H_S, in ‰ V-SMOW) profiles from Day of Experiment (DoE) 0–100 (top panel), from DoE 101–287 (middle panel), and from DoE 288–299 (bottom panel).
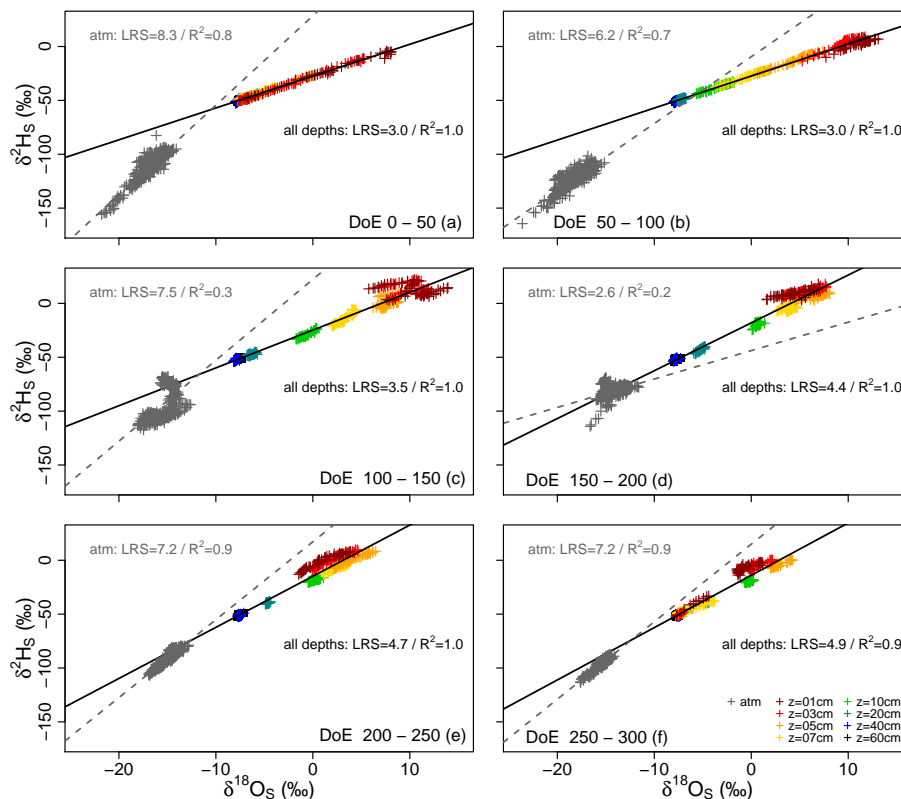
Figure 6. Linear regressions (gray dotted line) between laboratory atmosphere water vapor $\delta^{18}O$ and δ^2H (in ‰ V-SMOW) and between soil water $\delta^{18}O$ and δ^2H (solid black line). Each plot represents data from 50 consecutive days of experiment (DoE). Coefficient of correlation (R^2) as well as the slope of the linear regressions (LRS) are reported.

Full Screen / Esc

Printer-friendly Version

Interactive Discussion
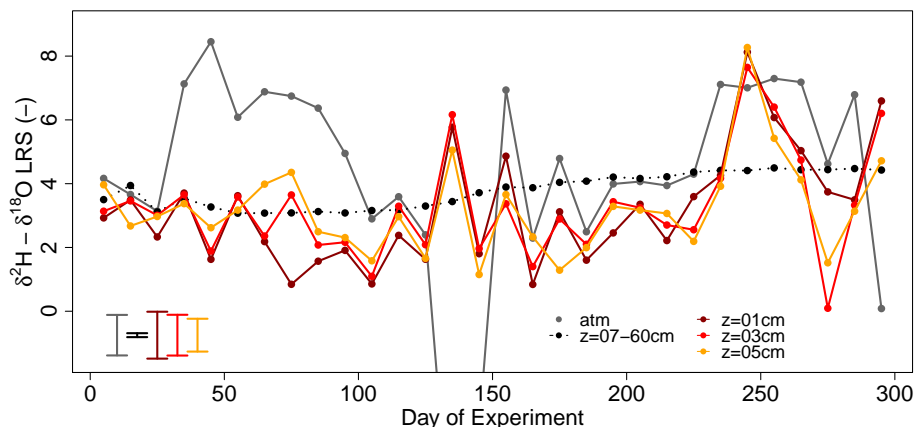
Figure 7. Time course of the slopes of the $\delta^{18}O$–δ^2H linear regressions (LRS) for time intervals of ten consecutive days of atmosphere data (gray solid line), soil data from the upper three layers (01, 03, and 05 cm, colored solid lines), and combined soil data from the remaining bottom layers (from 07 to 60 cm, black dotted line). Mean standard errors are represented by the error bars in the bottom left corner.
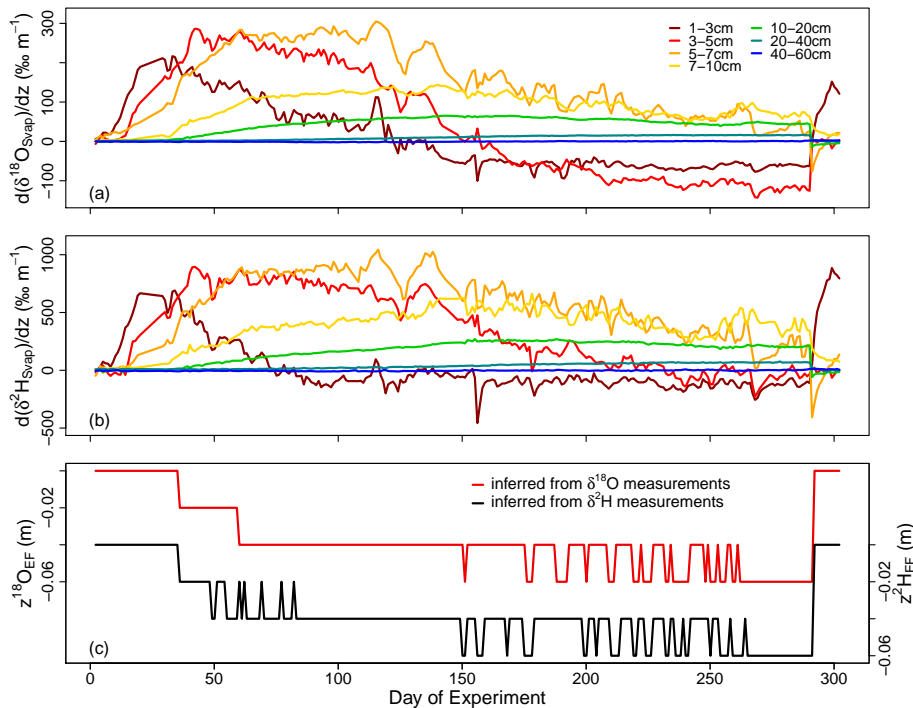
Figure 8. (a) and **(b)** $^{1}H^{2}H^{16}O$ and $^{1}H_{2}^{18}O$ composition gradients calculated between consecutive observation points in the soil. **(c)** Evolution of the evaporation front depths $z^{18}O_{EF}$ (red solid line) and $z^{2}H_{EF}$ (black solid line) inferred from the $^{1}H^{2}H^{16}O$ and $^{1}H_{2}^{18}O$ composition gradients.

Title Page

Abstract | Introduction

Conclusions | References

Tables | Figures

|◄ | ►|

◄ | ►

Back | Close

Full Screen / Esc